JCBFM

Journal of Cerebral Blood Flow & Metabolism
2017, Vol. 37(3) 1163–1178
© Author(s) 2017
Reprints and permissions:
sagepub.co.uk/journalsPermissions.nav
DOI: 10.1177/0271678X16685105
journals.sagepub.com/home/jcbfm
SAGE

PET imaging of cannabinoid type 2 receptors with [^{11}C]A-836339 did not evidence changes following neuroinflammation in rats

Geraldine Pottier[1], Vanessa Gómez-Vallejo[2], Daniel Padro[3], Raphaël Boisgard[1], Frédéric Dollé[1], Jordi Llop[2], Alexandra Winkeler[1] and Abraham Martín[4]

Abstract

Cannabinoid type 2 receptors (CB2R) have emerged as promising targets for the diagnosis and therapy of brain pathologies. However, no suitable radiotracers for accurate CB2R mapping have been found to date, limiting the investigation of the CB2 receptor expression using positron emission tomography (PET) imaging. In this work, we report the evaluation of the in vivo expression of CB2R with [^{11}C]A-836339 PET after cerebral ischemia and in two rat models of neuroinflammation, first by intrastriatal LPS and then by AMPA injection. PET images and in vitro autoradiography showed a lack of specific [^{11}C]A-836339 uptake in these animal models demonstrating the limitation of this radiotracer to image CB2 receptor under neuroinflammatory conditions. Further, using immunohistochemistry, the CB2 receptor displayed a modest expression increase after cerebral ischemia, LPS and AMPA models. Finally, [^{18}F]DPA-714-PET and immunohistochemistry demonstrated decreased neuroinflammation by a selective CB2R agonist, JWH133. Taken together, these findings suggest that [^{11}C]A-836339 is not a suitable radiotracer to monitor in vivo CB2R expression by using PET imaging. Future studies will have to investigate alternative radiotracers that could provide an accurate binding to CB2 receptors following brain inflammation.

Keywords

[^{11}C]A-836339, cannabinoid type 2 receptors, cerebral ischemia, [^{18}F]DPA-714, neuroinflammation, positron emission tomography, TSPO

Received 28 July 2016; Revised 23 November 2016; Accepted 25 November 2016

Introduction

The cannabinoid (CB) receptors are members of a superfamily G-protein coupled receptors involved in a variety of physiological processes including appetite, pain-sensation, mood and memory.[1] The primary receptors of the endocannabinoid system are the CB1 and CB2 cannabinoid receptors.[2] Despite CB1 receptors are predominantly expressed by neurons in the cortex, hippocampus, amygdale, basal ganglia and cerebellum,[3] CB2 receptors are abundant on immune cells regulating migration, cytokine production and antigen presentation.[4,5] In the central nervous system (CNS), CB2 receptors have been identified on microglial and dendritic cells demonstrating the role of these receptors in CNS inflammatory response.[6,7] Likewise, several preclinical

[1]Imagerie Moléculaire In Vivo, Inserm, CEA, Univ. Paris Sud, CNRS, Université Paris Saclay, CEA – Service Hospitalier Frédéric Joliot, Orsay, France
[2]Radiochemistry and Nuclear Imaging, CIC biomaGUNE, San Sebastian, Spain
[3]Magnetic Resonance Imaging, CIC biomaGUNE, San Sebastian, Spain
[4]Molecular Imaging Unit, CIC biomaGUNE, San Sebastian, Spain

Co-Corresponding authors:
Abraham Martín, Unidad de Imagen molecular, CICbiomaGUNE, Edificio Empresarial "C", Pº Miramon 182, San Sebastian, Spain.
Email: amartin@cicbiomagune.es
Alexandra Winkeler, Imagerie Moléculaire In Vivo, Inserm, CEA, Univ. Paris Sud, CNRS, Université Paris Saclay, CEA - Service Hospitalier Frédéric Joliot, Orsay, France.
Email: alexandra.winkeler@cea.fr

studies have shown the anti-inflammatory therapeutic potential of CB2 receptor activation in cerebral pathologies such as cerebral ischemia,[8–10] multiple sclerosis,[11,12] Alzheimer's disease,[13] Hungtinton's disease,[14,15] Parkinson's disease[16] and Amyotrophic lateral sclerosis.[17,18] The therapeutic mechanism involved responds to the ability of CB2 receptors to attenuate microglial activation and prevent neuronal degeneration in most of the CNS disorders.[2] In this context, the in vivo imaging of cannabinoid type 2 receptors (CB2R) with positron emission tomography (PET) might be crucial to further understand the role of these receptors on inflammatory reactions underlying brain diseases. Several PET radiotracers for CB2 receptors have been synthesized and tested preclinically, such as [^{11}C]KD2,[19] [^{11}C]RS-016,[20] [^{18}F]CB91,[21] [^{11}C]A-836339[22] and in human volunteers [^{11}C]NE40.[23] Among them, [^{11}C]A-836339 has been suggested as a promising radiotracer for the in vivo evaluation of a neuroinflammatory reaction in both a systemic lipopolysaccharide (LPS)-induced mouse model of neuroinflammation and a mouse model of Alzheimer's disease.[22] In contrast, [^{11}C]NE40 has not shown to be sensitive enough to visualize the CB2 receptor expression after cerebral ischemia in mice in part due to its low affinity for CB2 receptors.[24] Therefore, the purpose of the present study was to investigate cerebral CB2 receptor changes following the induction of two rat models of neuroinflammation using [^{11}C]A-836339 PET and immunohistochemistry. In particular, we were interested in determining the potential of this radiotracer to image CB2 expression following three well established animal models of neuroinflammation such as (i) transient focal cerebral ischemia,[25] (ii) LPS-induced[26] and (iii) α-amino-3-hydroxy-5-methyl-4-isoxazolepropionic acid (AMPA)-induced model in rats.[27] Further, [^{18}F]DPA-714, a radioligand specific for the translocator protein 18 kDa-TSPO (a well-known marker of neuroinflammation[28]) was used to evaluate the effect of a selective agonist for CB2 receptors (JWH133) on the inflammatory reaction after ischemic stroke in rats. Finally, the neurofunctional outcome was assessed to evaluate the usefulness of the treatment in stroke recovery.

Materials and methods

Animal models

Adult male Sprague-Dawley rats (n = 30) for stroke studies and Wistar rats (n = 10) for AMPA and LPS administration (300 g body weight; Janvier, France) were used. Animal experimental protocols and relevant details regarding welfare and drug side effects were approved by the animal ethics committee of CIC biomaGUNE and CEA and were conducted in accordance with the ARRIVE guidelines and Directives of the European Union on animal ethics and welfare.

Cerebral ischemia and treatment

Transient focal ischemia was produced by a 90-min intraluminal occlusion of the middle cerebral artery (MCA) followed by reperfusion as described previously.[29] Briefly, rats were anaesthetized with 2.5% isoflurane in 100% O_2 and a 2.6-cm length of 4–0 monofilament nylon suture was introduced into the right external carotid artery up to the level where the MCA branches out. Animals were then sutured and placed in their cages with free access to water and food. After 90 min, the animals were re-anesthetized and the filament was removed to allow reperfusion. Six rats were repeatedly examined before ischemia (day 0) and at 1, 3, 7, 14, 21 and 28 days afterwards to evaluate the temporal PET binding of CB2 receptors. The animals studied at day 0 have been considered as the baseline control group. A group of seven rats was inoculated daily for a total of seven days from one hour following MCAO with 0.1 mL JWH133 (in TocriSolve^{TM} 100) (1.5 mg/Kg, i.p.). A control ischemic group of five rats received the same volume of vehicle (normal saline) daily. At day seven, treated and control rats were imaged with PET to determine the effect of JWH133 on TSPO expression. Twelve rats were used to perform ex vivo studies (immunohistochemistry) for CB2 receptor expression at 0, 7 and 28 days after cerebral ischemia. Rats used in imaging studies for the assessment of the effect of the treatment were also used to perform immunohistochemistry for TSPO (n = 12). In total, MCAO was induced in 26 rats.

LPS and AMPA administration

Animals were were anaesthetized with 2.5% isoflurane in 100% O_2 and stereotactically injected with 1 μg lipopolysaccharide (LPS from Escherichia coli 055:B5, Sigma, 1 μg/μL in PBS buffer) (n = 4) or 0.5 μL of α-amino-3-hydroxy-5-methylisoxazole-4-propionic acid (AMPA, Sigma, 15 mM) (n = 2) using a 1 μL microsyringe (Hamilton) and a micropump (Micro4 Controller; WPI Inc.) into the right striatum (Bregma:+1.0 mm, lateral: −3.0 mm, depth: 4.0 mm from the surface of the brain). The infusion rate was set to 500 nL/min and the syringe was left in place for 10 min after injection before it was retracted slowly. The site of incision was then cleaned, and sutured using 4.0 braided silk before being disinfected. Animals were maintained normothermic during the surgery through the use of a heating blanket (Homeothermic Blanket Control Unit; Harvard Apparatus Ltd.). Six rats were used to perform in vivo PET imaging after LPS (n = 4) and

AMPA administration (n = 2) and four rats were used for ex vivo autoradiographic or immunohistochemical studies of LPS (n = 2) and AMPA (n = 2) models.

Magnetic resonance imaging

T2-weighted (T_2W) MRI scans were performed in ischemic animals at 24 h after reperfusion to select the rats (n = 6) presenting cortico-striatal lesions for inclusion in the PET studies. Before the scans, anesthesia was induced with 4% isoflurane and maintained by 2–2.5% of isofluorane in 100% O_2 during the scan. Animals were placed into a rat holder compatible with the MRI acquisition systems and maintained normothermic using a water-based heating blanket at 37°C. MRI experiments were performed on a 7 Tesla Bruker Biospec 70/30 MRI system (Bruker Biospin GmbH, Ettlingen, Germany), interfaced to an AVANCE III console. The BGA12-S imaging gradient (maximum gradient strength 400 mT/m switchable within 80 µs), an 82 mm inner diameter quadrature volume resonator for transition and surface rat brain coil for reception were used. T2W images were acquired with a RARE sequence with the following parameters: RARE factor 2, TR/TE = 4400/40 ms, FOV = 25 mm × 25 mm, ACQ Matrix = 256 × 256, Slice Thickness = 1 mm, 2 averages and 24 contiguous slices. Contiguous slices covering all the infarcted volume were acquired and fat suppression was used.

Radiochemistry

[^{11}C]A-836339 preparation. A-836339 ((Z)-*N*-(3-(2-methoxyethyl)-4,5-dimethylthiazol-2(3 H)-ylidene)-2,2,3,3-tetramethylcyclopropanecarboxamide) was labelled by reaction of the corresponding desmethylated precursor with [^{11}C]CH_3I. Carbon-11 was directly generated as [^{11}C]CH_4 in an IBA Cyclone 18/9 cyclotron and transferred to a TRACERlab FX_C Pro synthesis module (GE Healthcare, Waukesha, WI, USA), where [^{11}C]CH_3I was generated via the gas-phase method, distilled under continuous helium flow (20 mL/min) and introduced in a 2 mL stainless steel reaction loop precharged with a solution of (Z)-*N*-(3-(2-hydroxyethyl)-4,5-dimethylthiazol-2(3H)-ylidene)-2,2,3,3-tetramethylcyclopropanecarboxamide (1 mg) in dimethylformamide (80 µL) using potassium hydroxide as the base. The reaction was allowed to occur for 5 min at 25°C and the crude was then purified by means of high-performance liquid chromatography (HPLC) using a Luna C18 column (Phenomenex, Madrid, Spain) as the stationary phase and 0.1 M aqueous formic acid solution /methanol 22/78 (v/v) as the mobile phase. The collected fraction (retention time: 9–11 min) was reformulated by dilution with water (20 mL), retention on a C-18 cartridge (Sep-Pak® Light, Waters, Milford, MA, USA) and eluted with ethanol (1 mL) and saline (9 mL). Filtration through a 0.22-µm sterile filter yielded the final injectable solution. For quality control, a Mediterranean Sea18 column (Teknokroma, Barcelona, Spain) was used as stationary phase and 0.1 M aqueous formic acid solution/methanol 30/70 (v/v) as the mobile phase. Radiochemical yields and specific activities were 34 ± 4 % (end of bombardment) and 175 ± 8 GBq/µmol at injection time, respectively. Radiochemical purity was > 99% in all cases.

[^{18}F]DPA-714 preparation. The synthesis of [^{18}F]DPA-714 (*N,N*-diethyl-2-(2-(4-(2-[^{18}F]fluoroethoxy)phenyl)-5,7-dimethylpyrazolo[1,5-a]pyrimidin-3-yl)acetamide was performed using a TRACERlab FX_{FN} synthesis module (GE Healthcare), based on a one-step procedure, as previously described.[30,31] Briefly, once transferred into a dedicated (ventilated and lead-shielded) hot-cell, fluorine-18 as [^{18}F]fluoride (cyclotron-produced, IBA Cyclone 18/9) was first trapped on a pre-conditioned Sep-Pak® Accell Plus QMA Light cartridge (Waters, Milford, MA, USA), then eluted from the cartridge with a solution of Kryptofix K2.2.2/K_2CO_3 in a mixture of water and acetonitrile. A solution containing the appropriate tosyloxy precursor for labelling (*N,N*-diethyl-2-(2-(4-(2-toluenesulfonyloxyethoxy)phenyl)-5,7-dimethylpyrazolo[1,5-a]pyrimidin-3-yl)acetamide, 4 mg) in dimethylsulfoxide (0.7 mL) was added and the mixture heated at 165°C for 5 min. The reactor was then cooled at room temperature, the reaction crude diluted with a mixture of acetonitrile and water (2/1, 3 mL), and purified by HPLC using a Nucleosil 100-7 C18 column (Macherey-Nagel, Düren, Germany) as stationary phase and 0.1 M aqueous ammonium formate solution (pH = 3.9) / acetonitrile (30/70) as the mobile phase at a flow rate of 7 mL/min. The desired fraction (10–11 min) was collected, diluted with water (20 mL), and the radiotracer was retained on a C-18 cartridge (Sep-Pak® Light, Waters, Milford, MA, USA) and further eluted with ethanol (1 mL). The ethanol solution was finally reconstituted with saline solution (9 mL). Filtration through a 0.22-µm filter yielded the final solution, ready for injection. Radiochemical yields (non-decay corrected) were in the range 8–13% and radiochemical purity was always >95% at the time of injection. Radiochemical yields were 8–13% (end of bombardment) and specific activities ranged from 100 to 900 GBq/µmol at injection time, respectively. Radiochemical purity was >95% in all cases.

PET scans and data acquisition

Cerebral ischemia studies. PET scans were repeatedly performed before reperfusion (day 0) and at 1, 3, 7, 14, 21

and 28 days afterwards using a General Electric eXplore Vista CT camera (GE Healthcare). Scans were performed in rats anaesthetized with 4% isofluorane and maintained by 2–2.5% of isofluorane in 100% O_2. The tail vein was catheterized with a 24-gauge catheter for intravenous administration of the radiotracer. Animals were placed into a rat holder compatible with PET acquisition system and maintained normothermic using a water-based heating blanket. Animals were subjected to PET scans to assess CB2 receptors ([^{11}C]A-836339) at each time point (before and after ischemia onset). For longitudinal imaging evaluation of CB2 receptors, ~70 MBq of [^{11}C]A-836339 was injected at the start of the PET acquisition. Dynamic brain images were acquired (24 frames: 1×5, 1×15, 3×30, 5×60, 4×120, 4×180, 6×300 s) in the 400–700 keV energetic window, with a total acquisition time of 57.5 min. For evaluation of JWH133 treatment efficacy after ischemia, ~70 MBq of [^{18}F]DPA-714 were injected at the start of the PET acquisition and dynamic brain images were acquired for a total of 30 min (23 frames 3×5, 3×15, 4×30, 4×60, 4×120, 5×180 s). After each PET scan, CT acquisitions were also performed (140 μA intensity, 40 kV voltage), providing anatomical information of each animal as well as the attenuation map for the later image reconstruction. Dynamic acquisitions were reconstructed (decay and CT-based attenuation corrected) with filtered back projection (FBP) using a Ramp filter with a cutoff frequency of 0.5 mm^{-1}.

LPS and AMPA studies. [^{11}C]A-836339 dynamic PET scans were acquired two days (LPS) or seven days (AMPA) after intrastriatal injection using a Siemens Inveon® small animal PET or PET-CT scanner. Both scanners were used in parallel in order to assure a high specific radioactivity at the time of injection. The imaging time points were chosen based on previous studies that demonstrated different dynamics of the models which indicated strong neuroinflammation at early times (16–72 h) after LPS injection[26,32] compared to seven days post AMPA injection.[33] Animals were anaesthetized with isoflurane (induction: 4%, maintenance: 2–2.5%) in oxygen. The radiolabeled compound was injected in the caudal vein through a 24-gauge catheter at the start of the PET acquisition. The mean injected doses were ~40 MBq and PET data were acquired during 60 min. The acquisition protocol used the following parameters: the time coincidence window was set to 3438 ns and the levels of energy discrimination were set to 350 and 650 keV. The list-mode acquired data files were histogrammed into 3D sinograms with a maximum ring difference of 79 and span of 3. The list-mode data were sorted into 24 dynamic frames (3×30; 5×60; 5×120; 3×180; 3×240; 4×300 and 1×150 seconds). Finally, the emission sinograms (i.e. each frame) were normalized, corrected for scatter, attenuation and radioactivity decay and reconstructed using Fourier rebinning (FORE) and ordered subset expectation maximization (OSEM) 2D (16 subsets and 4 iterations). To acquire attenuation correction factors, a CT (Inveon® PET-CT) or a transmission scan using an external ^{68}Ge point source (Inveon® PET) was performed immediately prior to the PET scan for each animal.

PET image analysis

Cerebral ischemia studies. PET images were analyzed using PMOD image analysis software (PMOD Technologies Ltd, Zürich, Switzerland). To verify the anatomical location of the signal, PET images were co-registered to the anatomical data of an MRI rat brain template. VOIs were manually drawn in the entire ipsilateral hemisphere that contained the area supplied by the MCA on slices of a MRI (T_2W) rat brain template from the PMOD software to study the [^{11}C]A-836339 and [^{18}F]DPA-714 PET signal. For quantification of radiotracers uptake, the last three ([^{11}C]A-836339) or four frames ([^{18}F]DPA-714) in steady state were used to calculate the summed PET binding during the last 15 min of acquisition. PET signal uptake was averaged in each ROI and expressed as percentage of injected dose per cubic centimetre (% ID/cc).

LPS and AMPA studies. PET image analysis was performed using VINCI, a fast graphical image analysis package[34] with image co-registration tools. PET images were co-registered to an MRI template.[35] The Anatomist BrainVISA software package (http://www.brainvisa.info) was also used for data evaluation. For quantitative analysis, a volume-of-interest (VOI) analysis was performed on kinetic image data sets. Two VOIs were manually delineated, one around the injection site in the ipsilateral and one control VOI in the contralateral hemisphere. The time activity curves extracted from these VOIs were obtained from dynamic PET data and normalized by the injected dose (% ID).

Immunohistochemistry and cell counts. Immunohistochemistry staining was performed at control (day 0), day 7 and day 28 after cerebral ischemia. Animals were terminally anesthetized, killed by decapitation; the brain was removed, frozen and cut in 5-μm-thick sections in a cryostat. Sections were fixed in acetone (−20°C) during 2 min, washed with phosphate-buffered saline (PBS), saturated with a solution of bovine serum albumin (BSA) 5%/Tween 0.5% in PBS during 15 min at room temperature, and incubated during 1 h at room temperature with primary antibodies BSA (5%)/Tween

(0.5%) in PBS. The first set of sections were stained for CB2 with rabbit anti-rat CB2 (1:500, AbCam, Cambridge, UK), for CD11b with mouse anti-rat CD11b (1:300; Serotec, Raleigh, NC, USA) and for Iba1 with goat anti-rat Iba1 (1:500, AbCam, Cambrige, UK). Sections were washed (3×10 min) in PBS and incubated for 1 h at room temperature with secondary antibodies Alexa Fluor 488 goat anti-rabbit IgG and Alexa Fluor 594 goat anti-mouse IgG (Molecular Probes, Life Technologies, Madrid, Spain, 1:1000) and Alexa Fluor 546 donkey anti-goat IgG in BSA 5%/Tween 0.5% in PBS, washed again (3×10 min) in PBS, and mounted with a prolong with DAPI antifade kit in slices (Molecular Probes Life Technologies, Madrid, Spain). The second set of sections was stained for TSPO with a rabbit anti-rat TSPO (NP155, 1:1000), for CD11b (1:300; Serotec, Raleigh, NC, USA) and for the glial fibrillary acidic protein (GFAP) with chicken anti-rat GFAP (1:500; AbCam, Cambridge, UK). Sections were washed (3×10 min) in PBS and incubated for 1 h at room temperature with secondary antibodies Alexa Fluor 350 goat anti-rabbit IgG, Alexa Fluor 594 goat anti-mouse IgG and Alexa Fluor 488 goat anti-chicken IgG (Molecular Probes, Life Technologies, Madrid, Spain, 1:1,000) in BSA 5%/Tween 0.5% in PBS, washed again (3×10 min) in PBS, and mounted with a prolong antifade kit in slices (Molecular Probes Life Technologies, Madrid). Standardized images acquisition was performed with an Axio Observer Z1 (Zeiss, Le Pecq, France) equipped with a motorized stage. The number of microglial and astrocytic cells immunopositive for CB2 and CD11b within the ischemic area was assessed at 0, 7 and 28 days after ischemia ($CB2^+/CD11b^+$) and at day 7 to evaluate the inflammatory effect of CB2R inhibition ($TSPO^+/CD11b^+$ and $TSPO^+/GFAP^+$). Cells were manually counted in 10 representative and different fields at $100 \times$ magnification by using Image J (NIH) software.

Autoradiography. [^{11}C]A-836339 (12 GBq/μmol; 50 nM) and [^{18}F]DPA-714 (68G Bq/μmol; 3 nM) autoradiographic studies were performed using 10-μm brain sections. Specific binding was assessed using an excess (20 μM) of either unlabeled A-836339 or DPA-714, respectively. Briefly, sections were incubated for 20 min in Tris Buffer (50 mM TRIZMA preset crystals purchased from Sigma-Aldrich) adjusted to pH 7.4 with NaCl. The unbound excess ligands were removed by two 2-min wash cycles in cold buffer and then a final rinse in cold deionized water. Sections were then placed in direct contact with a Phosphor-Imager screen (Molecular Dynamics, Sunnyvale, CA) and exposed overnight. Autoradiograms in the ipsilateral hemisphere were analyzed using ImageJ (NIH) software.

Neurological assessment. The assessment of neurological outcome induced by cerebral ischemia was based on a previously reported 9-neuroscore test.[36] Four consecutive tests were performed on ischemic animals submitted to longitudinal imaging studies at 0, 1, 3, 7, 14, 21 and 28 days, and before (day 0) and at day 7 after ischemia in treated rats as follows: (a) spontaneous activity (moving and exploring = 0, moving without exploring = 1, no moving = 2); (b) left drifting during displacement (none = 0, drifting only when elevated by the tail and pushed or pulled = 1, spontaneous drifting = 2, circling without displacement or spinning = 3), (c) parachute reflex (symmetrical = 0, asymmetrical = 1, contralateral forelimb retracted = 2), and (d) resistance to left forepaw stretching (stretching not allowed = 0, stretching allowed after some attempts = 1, no resistance = 2). Total score could range from 0 (normal) to a 9 (highest handicap) point-scale.

Statistical analyses. Binding values within the ipsilateral hemisphere were averaged and compared with the averaged baseline control values (before MCAO) using one-way ANOVA analysis of variance followed by Dunnett's multiple comparison tests for post hoc analysis. Likewise, cellular expression of both microglial/CB2 receptors before ischemia (day 0) and at days 7 and 28 afterwards was compared using the same statistical analysis as for the PET imaging. An unpaired *t*-test was used to compare in vivo [^{11}C]A-836339 uptake values within the ipsilateral versus the contralateral hemisphere of LPS- and AMPA-injected animals and in vitro autoradiographic studies for [^{11}C]A-836339 and [^{18}F]DPA-714 binding in the ipsilateral hemisphere. The effect of JWH133 in ischemic rats was compared to control infarcted rats using an unpaired *t*-test. Finally, neurological outcome comparisons before and at day 7 after ischemia were performed using Mann–Whitney U-test. The level of significance was set at $p < 0.05$. Statistical analyses were performed with Graph Pad Prism software, version 5 (La Jolla, CA, USA).

Results

[^{11}C]A-836339 PET after cerebral ischemia

The levels and distribution of cannabinoid CB2 receptors were observed by PET imaging after 90 min MCAO and 1–28 days reperfusion in rats. The coronal brain images with normalized color scale shown in Figure 1 illustrate the [^{11}C]A-836339-PET uptake signals in ischemic rats at control (day 0) and then at 7, and 28 days after reperfusion (Figure 1(a), (c) and (d)). The extent of brain damage after cerebral ischemia was

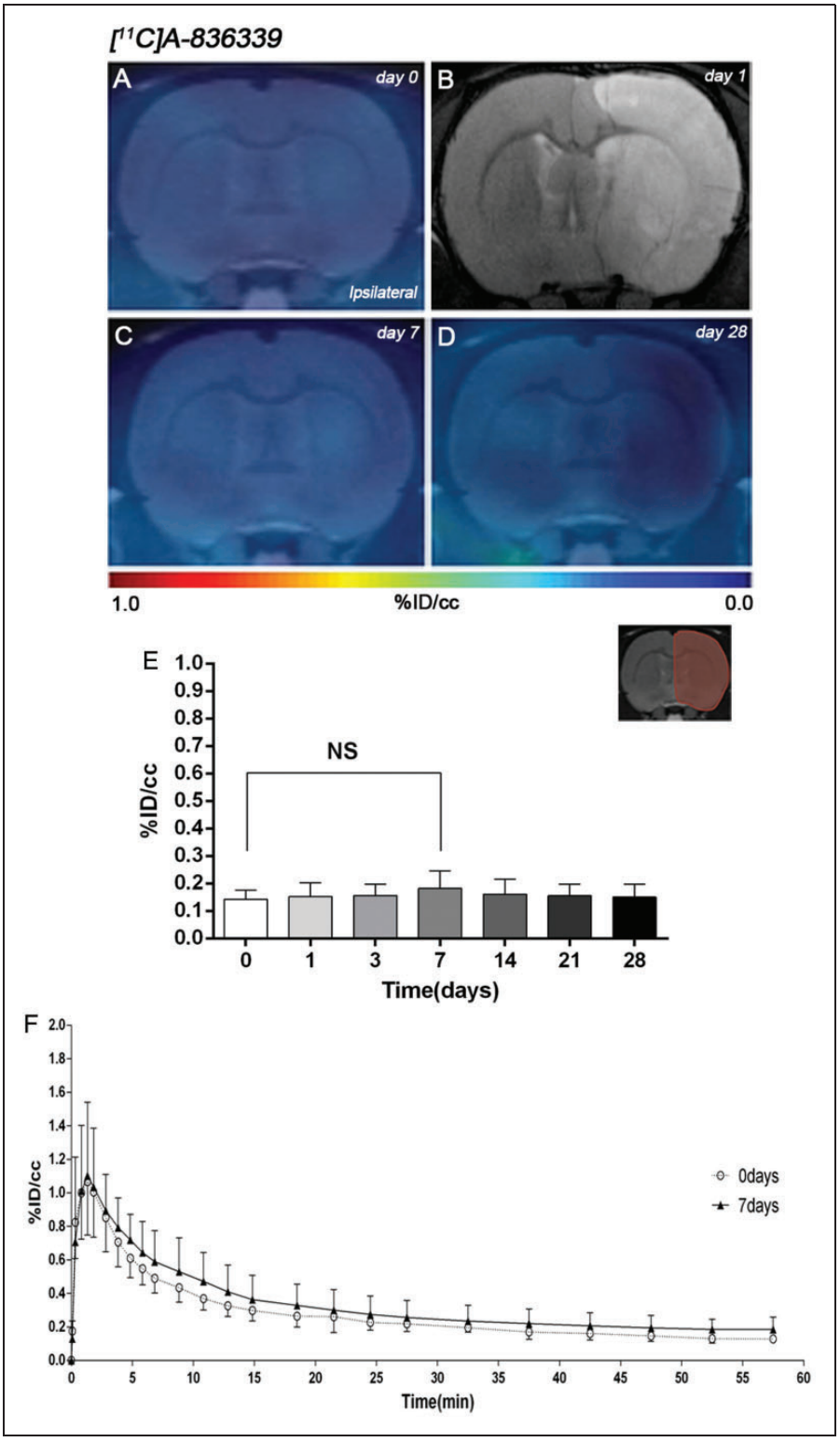

Figure 1. Time course of the progression of [^{11}C]A-836339 signal before and after middle cerebral artery occlusion (MCAO). The brain lesion at day 1 after reperfusion is shown with magnetic resonance imaging (MRI) alterations in T_2-weighted (T_2W) signal (b). Serial CB2 receptors PET binding images of coronal planes at control (day 0) (a), day 7 (c) and day 28 (d) after reperfusion. PET images are co-registered with a MRI (T_2W) template to localize the PET signal. Images are generated by averaging all PET frames and correspond to the lesion evolution of the same animal over time. (e) %ID/cc (mean $\pm$ SD) of [^{11}C]A-836339 was quantified in the entire ipsilateral cerebral hemisphere. The upper right panel shows the selected brain ROI for the quantification defined on a slice of a MRI (T2W) template. Rats ($n = 6$) were repeatedly examined by PET before (day 0) and at 1, 3, 7, 14, 21 and 28 after ischemia. (f) Time activity curves of [^{11}C]A-836339 binding in the ipsilateral hemisphere at days 0 and 7 following cerebral ischemia.

assessed using T2W-MRI at one day after ischemia onset (Figure 1(b)). Hyperintensities of T2W images showed similar infarct extents as well as locations affected. All ischemic rats who underwent nuclear imaging studies showed cortical and striatal MRI alterations (mean ± s.d. 357.64 ± 45.47 mm^3, $n = 6$). Quantification of the PET images provided information related to the time-course activity of CB2 receptors in the ipsilateral hemisphere at days 0 (control) and 1, 3, 7, 14, 21 and 28 days after MCAO (Figure 1(e), $n = 6$). In the infarcted hemisphere, the PET signal for [^{11}C]A-836339 showed a non-significant mild uptake increase during the first week followed by a slight decrease from days 14 to 28 after cerebral ischemia in rats (Figure 1(e)). The time-activity curves (TACs) generated in the ischemic cerebral hemisphere at days 0 and 7 after ischemia showed that [^{11}C]A-836339 uptake reached a peak value of radioactivity at few minutes after bolus injection followed by a fast wash-out during the following 15 min. Likewise, the radiotracer uptake reached a plateau level from 30 to 60 min after bolus injection. PET uptake at day 7 showed a non-significant difference in comparison to control animals (Figure 1(f)).

Expression of cannabinoid CB2 receptor in microglia after MCAO

Immunofluorescence staining exhibited CB2 expression in microglia/macrophages after ischemia (Figure 2). At day 7, cells with the morphology of amoeboid reactive microglia/macrophages showed intense CD11b immunoreactivity in the lesion (in red; Figure 2(a)) followed by a decrease at day 28 (in red; Figure 2(a)). In contrast, CB2 receptor immunoreactivity showed a mild increase at days 7 to 28 after cerebral ischemia (in green; Figure 2(b)). DAPI labeling displayed similar cellular density before and after MCAO (in blue; Figure 2(c)). Only few microglial cells expressing CD11b showed expression of CB2 receptor at days 7 and 28 after ischemia (in red and green; Figure 2(d) and (e)).

[^{11}C]A-836339 PET after LPS and AMPA injection

The levels and distribution of cannabinoid CB2 receptor were observed by PET imaging at days 2 and 7 after LPS (Figure 3) and AMPA (Figure 4) injection in rats, respectively. The coronal brain images with normalized color scale shown in Figures 3(a) and 4(a) display the [^{11}C]A-836339-PET uptake at day 2 after LPS (Figure 3(a)) and day 7 after AMPA injection (Figure 4(a)). The TACs generated in the ipsilateral and contralateral striatum after LPS (Figure 3(b), $n = 4$) and AMPA (Figure 4(b), $n = 2$) injection showed a peak uptake of [^{11}C]A-836339 at few minutes after bolus injection followed by a fast wash-out later on. The results showed only low retention of [^{11}C]A-836339 after both LPS and AMPA injection in the injured striatum. Indeed, similar signal levels were observed in both ipsilateral and contralateral striatum after neuroinflammation induced by LPS and AMPA injection.

Expression of cannabinoid CB2 receptor in microglia after LPS and AMPA injection

Immunofluorescence staining exhibited CB2 expression in microglia/macrophages after LPS (Figure 3) and AMPA (Figure 4) administration. At day 2 after LPS and day 7 after AMPA injection, cells with the morphology of amoeboid reactive microglia/macrophages showed intense Iba1 immunoreactivity in the lesion (in red; Figures 3(c) and 4(c)). In contrast, CB2 receptor immunoreactivity showed a very low signal in the injured region of both animal models (in green; Figures 3(d) and 4(d)). DAPI labeling displayed similar cellular density after LPS and AMPA injection (in blue; Figures 3(e) and 4(e)). Likewise, only few microglial cells expressing Iba1 showed expression of CB2 receptor at days 2 and 7 after LPS and AMPA administration (in red and green; Figures 3(f) and 4(f)).

In vitro autoradiograhy of [^{11}C]A-836339 and [18F]DPA-714 after LPS and AMPA injection

The evaluation of [^{11}C]A-836339 binding was performed on brain sections of rats sacrificed at days 2 and 7 after LPS and AMPA administration, respectively, to verify the results obtained with PET. [^{11}C]A-836339 binding showed no significant increase in the ipsilateral hemisphere relative to non-injured hemisphere after LPS and AMPA models (data not shown) supporting the results obtained by in vivo imaging. Despite this, the displacement studies using A-836339 showed a significant binding decrease in the ipsilateral hemisphere after LPS and AMPA injection ($p < 0.01$, Figure 5(a) and (b) and $p < 0.001$ Figure (g)). Moreover, [^{11}C]A-836339 binding was evaluated in the spleen as a potential positive control as Horti et al.[22] have shown binding accumulation using the same radiotracer. [^{11}C]A-836339 binding in spleen showed a 3-fold increase in comparison to LPS and AMPA lesions ($p < 0.001$, Figure 5(e) and (g)) supporting these previous results. Likewise, the [^{11}C]A-836339 displacement with A-836339 displayed a significant binding decrease in the rat spleen ($p < 0.001$, Figure 5(f) and (g)). The second set of experiments was performed to verify the existence of brain lesion after LPS and AMPA injection

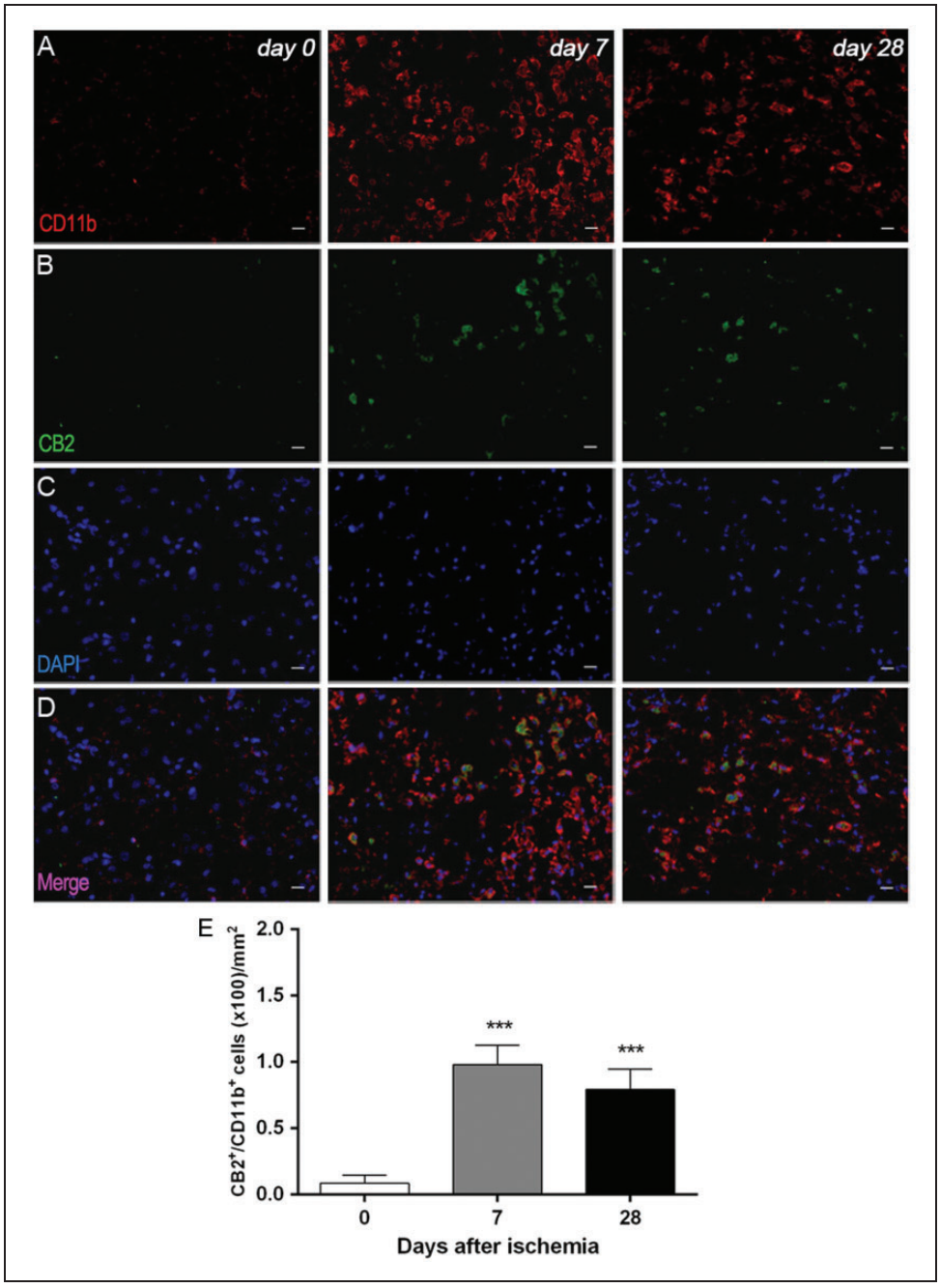

Figure 2. Immunofluorescent labeling of CD11b (red), CB2 (green), and DAPI (blue) in the ischemic area, shown as three channels. The data show temporal evolution of microglia expressing CB2 at day 0 (control) (left column, n = 4), day 7 (middle column, n = 4) and day 28 (right column, n = 4) after ischemia. (a) CD11b-reactive microglia/macrophages increase at days 7 to 28 (b) corresponding to the temporal CB2 immunoreactivity after ischemia (b). (c) DAPI labeling evidence similar cellular density before and after MCAO. (d) Merged images of three immunofluorescent channels at different time points. The number of CD11b-reactive microglia/macrophages expressing CB2 receptor increases in the ischemic area following ischemia (e). Scale bars, 20 μm. ***$p < 0.001$ compared with day 0.

by using [^{18}F]DPA-714, a specific radiotracer for neuroinflammation. In both animal models, [^{18}F]DPA-714 uptake was observed and highly reduced after displacement studies with cold DPA-714 which demonstrates a high TSPO expression. In the present experiment, LPS injected rats showed a significant [^{18}F]DPA-714 uptake increase in comparison to AMPA administration ($p < 0.05$, Figure 5(c), (d) and (h)).

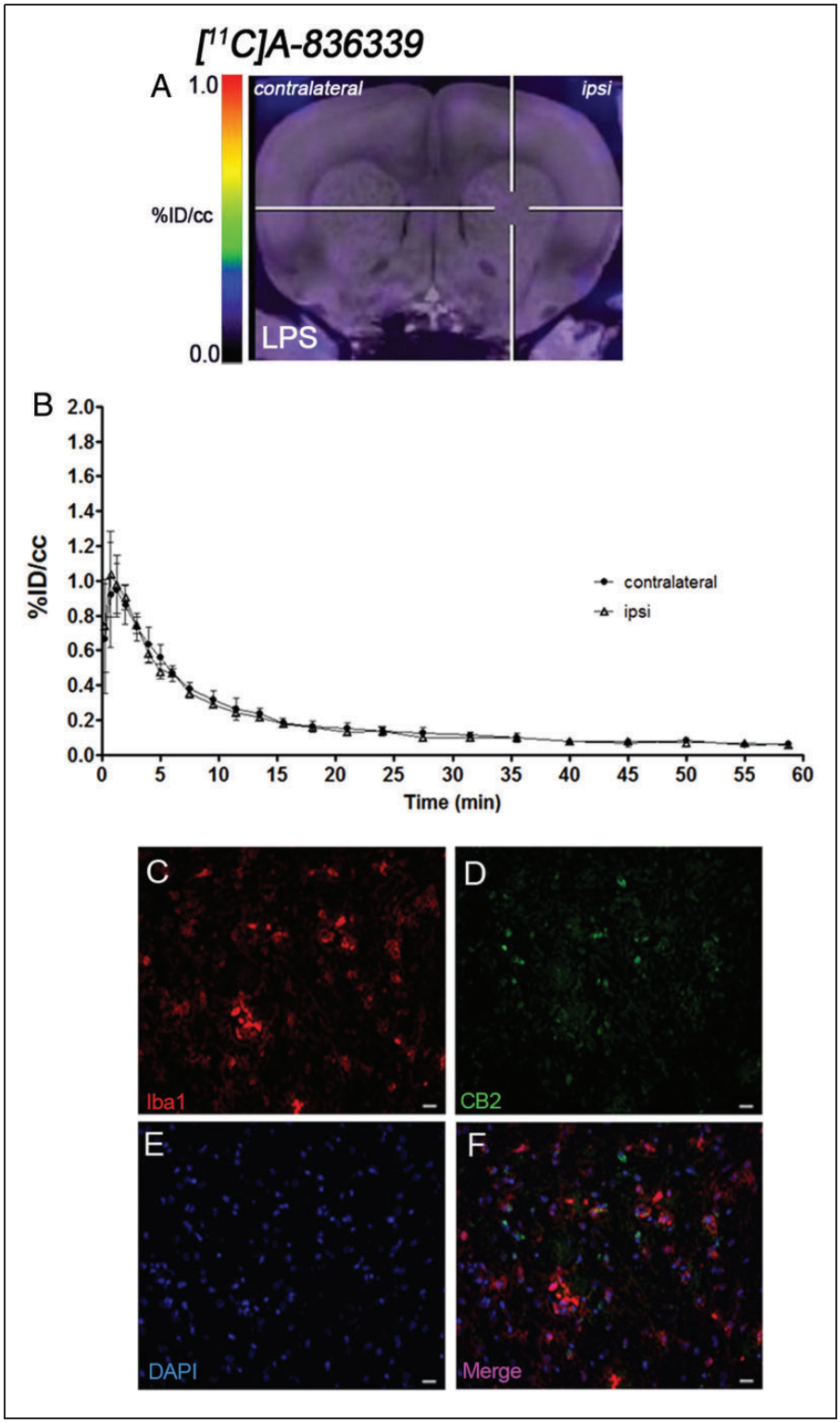

Figure 3. CB2 receptor binding with [^{11}C]A-836339 PET at day 2 after LPS administration. (a) [^{11}C]A-836339 PET image is co-registered with a MRI (T_2W) template to localize the PET signal. The hairlines indicate the location of the injection site. PET image is generated by averaging all frames. (b) Average time activity curves of [^{11}C]A-836339 binding at day 2 for VOIs placed in the ipsilateral and contralateral striatums after LPS injection. Immunofluorescent labeling of Iba1 (a), CB2 (b), DAPI (b) and the merge of the three channels (f). Scale bars, 20 μm.

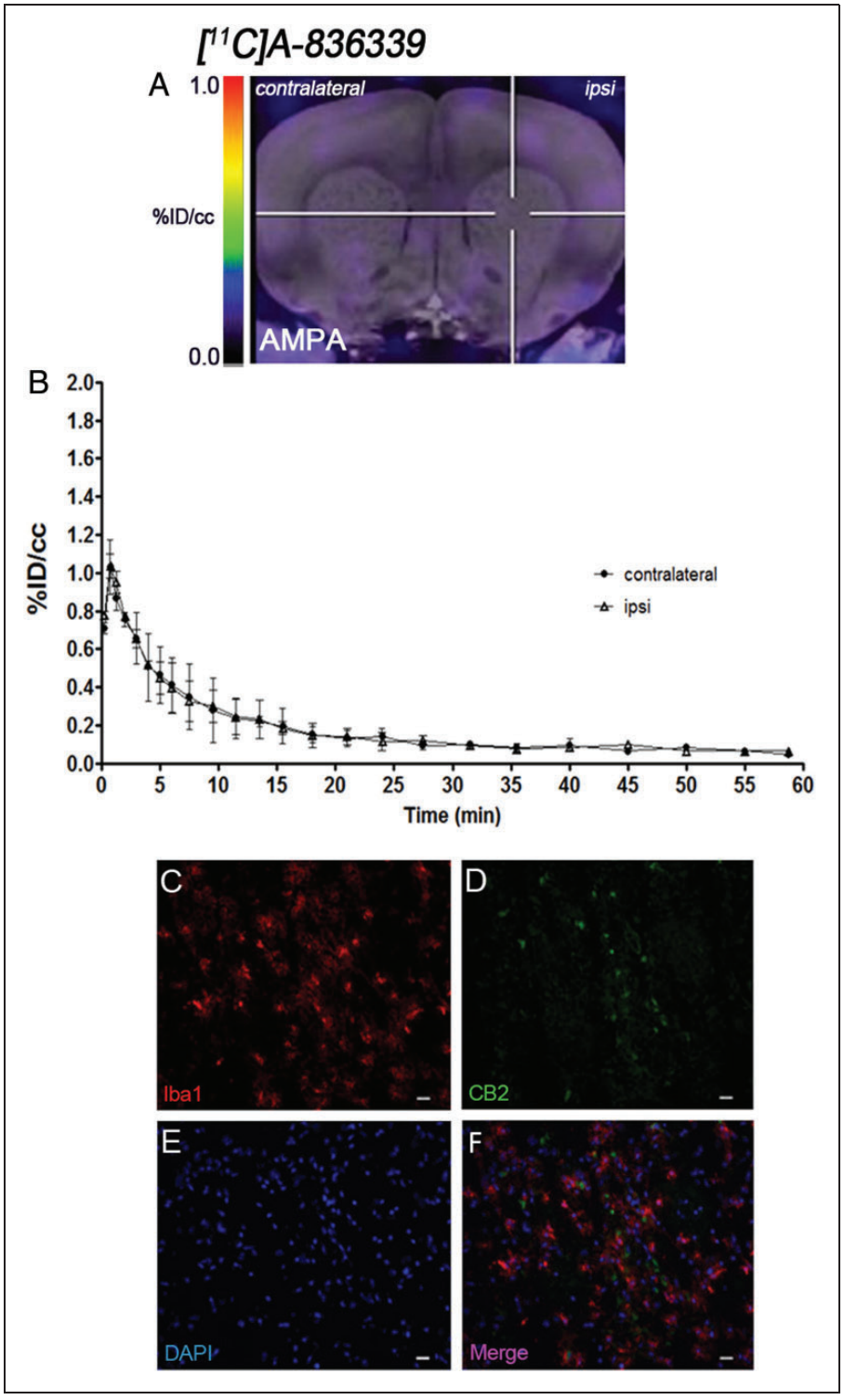

Figure 4. CB2 receptor binding with [^{11}C]A-836339 PET at day 7 after AMPA administration. (a) [^{11}C]A-836339 PET image is co-registered with a MRI (T_2W) template to localize the PET signal. The hairlines indicate the location of the injection site. PET image is generated by averaging all frames. (b) Average time activity curves of [^{11}C]A-836339 binding at day 7 for VOIs placed in the ipsilateral and contralateral striatums after AMPA injection. Immunofluorescent labeling of Iba1 (a), CB2 (b), DAPI (b) and the merge of the three channels (f). Scale bars, 20 μm.

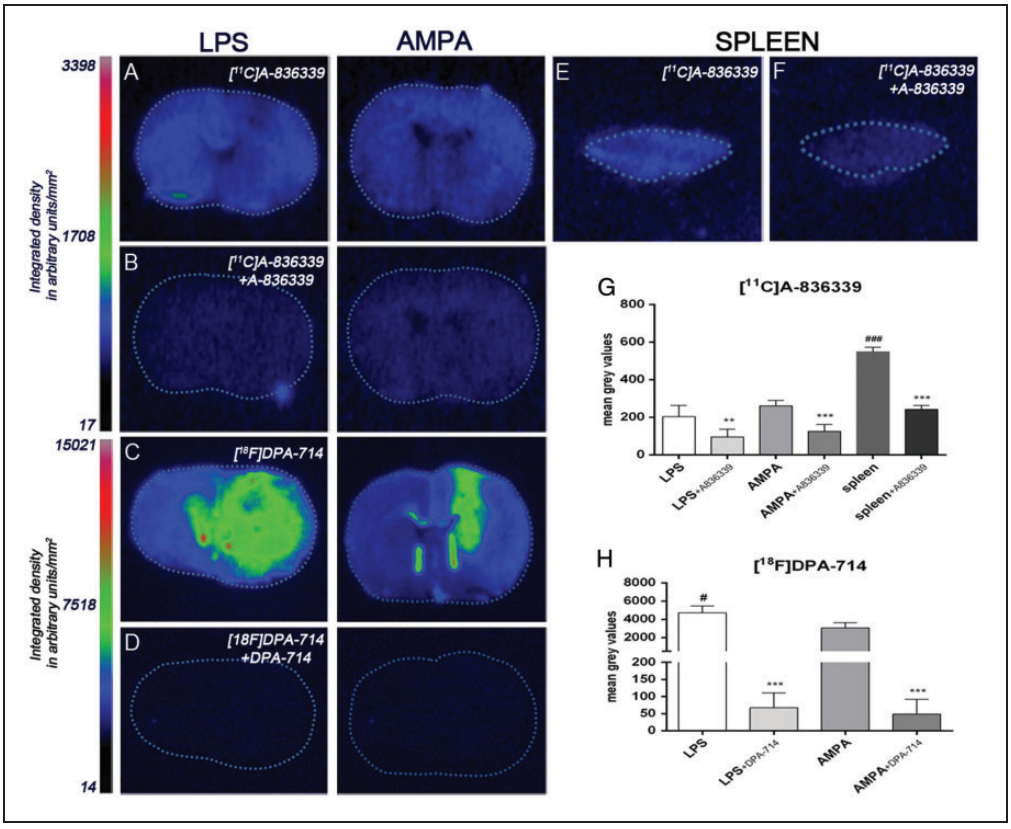

Figure 5. Autoradiograms of coronal brain sections after LPS and AMPA administration (a–d). The adjacent brain sections at the level of striatum show CB2 binding with [^{11}C]A-836339 (a), [^{11}C]A-836339 displacement with A-836339 (b) and the TSPO binding with [^{18}F]DPA-714 (c) and [^{18}F]DPA-714 displacement with DPA-714 (d) for both animal models. Autoradiograms of a section of rat spleen as positive control show CB2 binding with [^{11}C]A-836339 (E) and [^{11}C]A-836339 displacement with A-836339 (f). In vitro autoradiographic measures show [^{11}C]A-836339 binging after LPS (n = 6), LPS + A-836339 (n = 6), AMPA (n = 6), AMPA + A-836339 (n = 6), spleen (n = 3), spleen + A-836339 (n = 3) (g) and [^{18}F]DPA-714 binding after LPS (n = 3), LPS + DPA-714 (n = 3), AMPA (n = 3) and AMPA + DPA-714 (n = 3) (h). $^{**}p < 0.01$ and $^{***}p < 0.001$ compared with no displacement; $^{\#}p < 0.05$ and $^{\#\#\#}p < 0.001$ compared with AMPA, and AMPA/LPS, respectively.

Effect of CB2 receptor activation on neuroinflammation following cerebral ischemia

The effect of CB2 receptor activation with JWH133 on neuroinflammation was explored using PET [^{18}F]DPA-714 PET imaging at day 7 following MCAO (Figure 6). All the images were quantified in standard units, i.e. % ID/cc. Coronal and axial images with normalized color scale illustrate the [^{18}F]DPA-714 PET uptake in non-treated (MCAO + vehicle) (Figure 6(a) and (b)) and treated (MCAO + JWH133) (Figure 6(c) and (d)) ischemic rats. JWH133 treatment showed a significant decrease of [^{18}F]DPA-714 binding in the ischemic cerebral hemisphere compared to non-treated ischemic rats ($p < 0.05$, Figure 6(e)). In contrast, the contralateral hemisphere showed similar [^{18}F]DPA-714 binding in both treated and non-treated ischemic rats (Figure 6(e)). Furthermore, the ischemic striatum showed a non-significant higher retention of [^{18}F]DPA-714 relative to the cortical area in both treated and non-treated ischemic rats (Figure 6(f)). JWH133 treatment showed a significant decrease of [^{18}F]DPA-714 signal uptake in the ischemic striatum and a non-significant reduction in cerebral cortex in comparison to non-treated ischemic rats ($p < 0.05$, Figure 6(f)). Neurological score at day 1 after ischemia showed similar values reflecting that the groups presented similar neurological impairment before the start of the treatments (Figure 6(g)). At day 7, ischemic rats treated with JWH133 displayed a similar neurofunctional improvement compared to that seen in non-treated ischemic rats ($p < 0.01$, Figure 6(g)).

Expression of TSPO receptors in microglia and astrocytes after treatments in ischemic rats

Immunofluorescence staining exhibited TSPO expression (Figure 7(c)) in both microglia/macrophages (Figure 7(b)) and astrocytes (Figure 7(a)) after ischemia in non-treated and treated-rats. At day 7, cells with

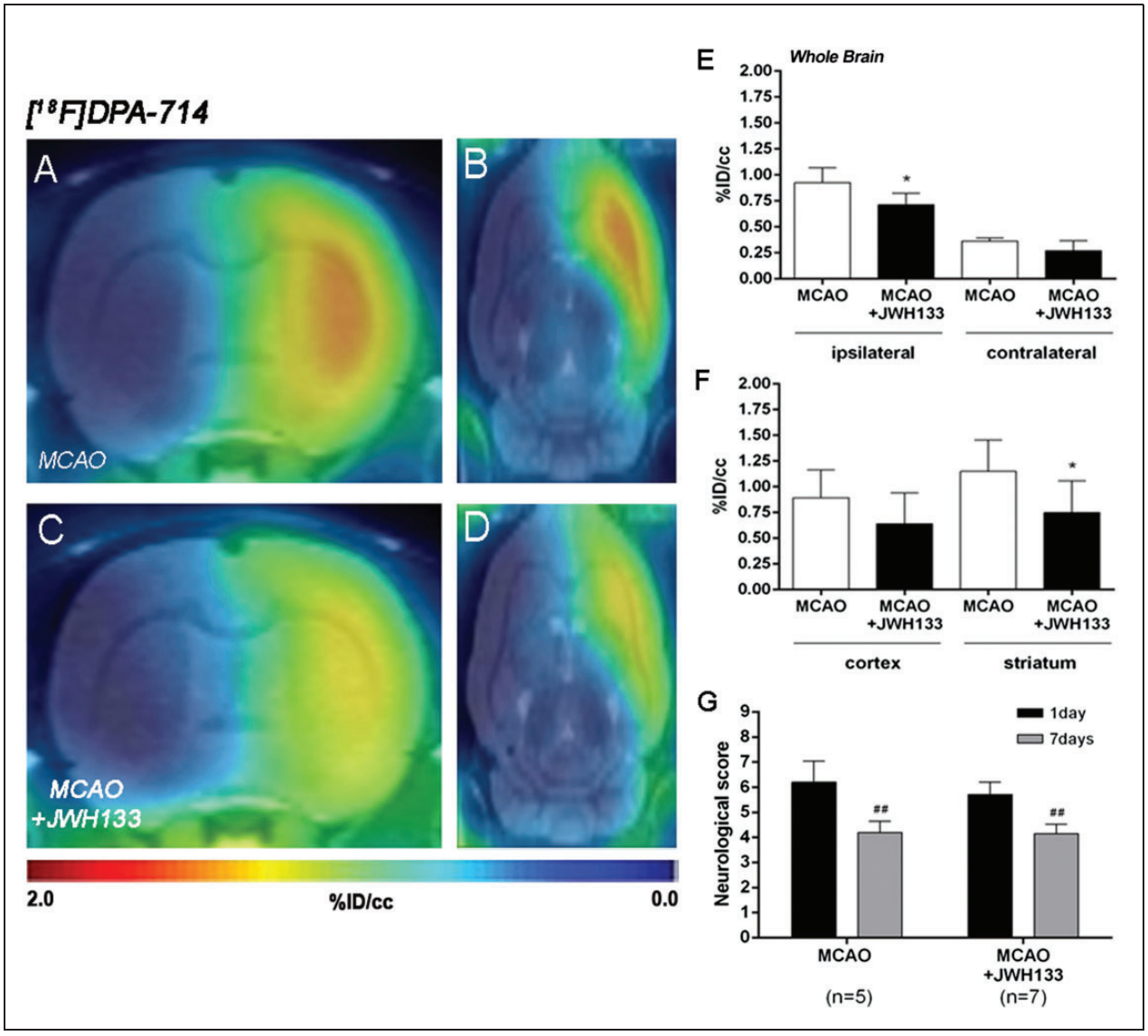

Figure 6. Normalized coronal (a, c) and axial (b, d) PET images of [^{18}F]DPA-714 at day 7 after middle cerebral artery occlusion (MCAO) in vehicle (a, b) and JWH133 (c, d) rats. PET images are co-registered with a MRI (T_2W) rat template to localize anatomically the PET signal. [^{18}F]DPA-714 uptake was quantified in vehicle ($n = 5$) and JWH133 ($n = 7$) at day 7 after ischemia as %ID/cc (mean ± SD) in the cerebral hemispheres, cortex and striatum (e–f). The neurologic score shows similar neurologic outcome at day 1 after ischemia (before the start of treatment) followed by a neurological outcome improvement at day 7 after cerebral ischemia (g). $^{*}p < 0.05$ compared with vehicle; $^{\#\#}p < 0.01$ compared with day 1.

the morphology of amoeboid reactive microglia/macrophages showed intense CD11b immunoreactivity (in red; Figure 7(b)) in the lesion that co-localized with TSPO receptor expression (in green and red; Figure 7(d)). The number of TSPO^{+}/CD11b^{+} cells displayed a significant decrease in treated ischemic rats with JWH133 at day 7 after ischemia in comparison with control ischemic rats ($p < 0.01$, Figure 7(e)). In contrast, equivalent number of TSPO^{+}/GFAP^{+} cells was observed for non-treated and treated ischemic rats at seven days after ischemia (Figure 7(f)).

Discussion

During recent years, cannabinoid CB2 receptors have emerged as promising targets for the diagnosis and therapy of neurological and neurodegenerative pathologies. Preclinical studies have shown that the CB receptor system might exert a neuroprotective effect over a large number of neurological and neurodenerative disorders.[8–18] Despite this, the application of CB-based medicines into the clinical use is still a major challenge for the near future. The evaluation of promising novel

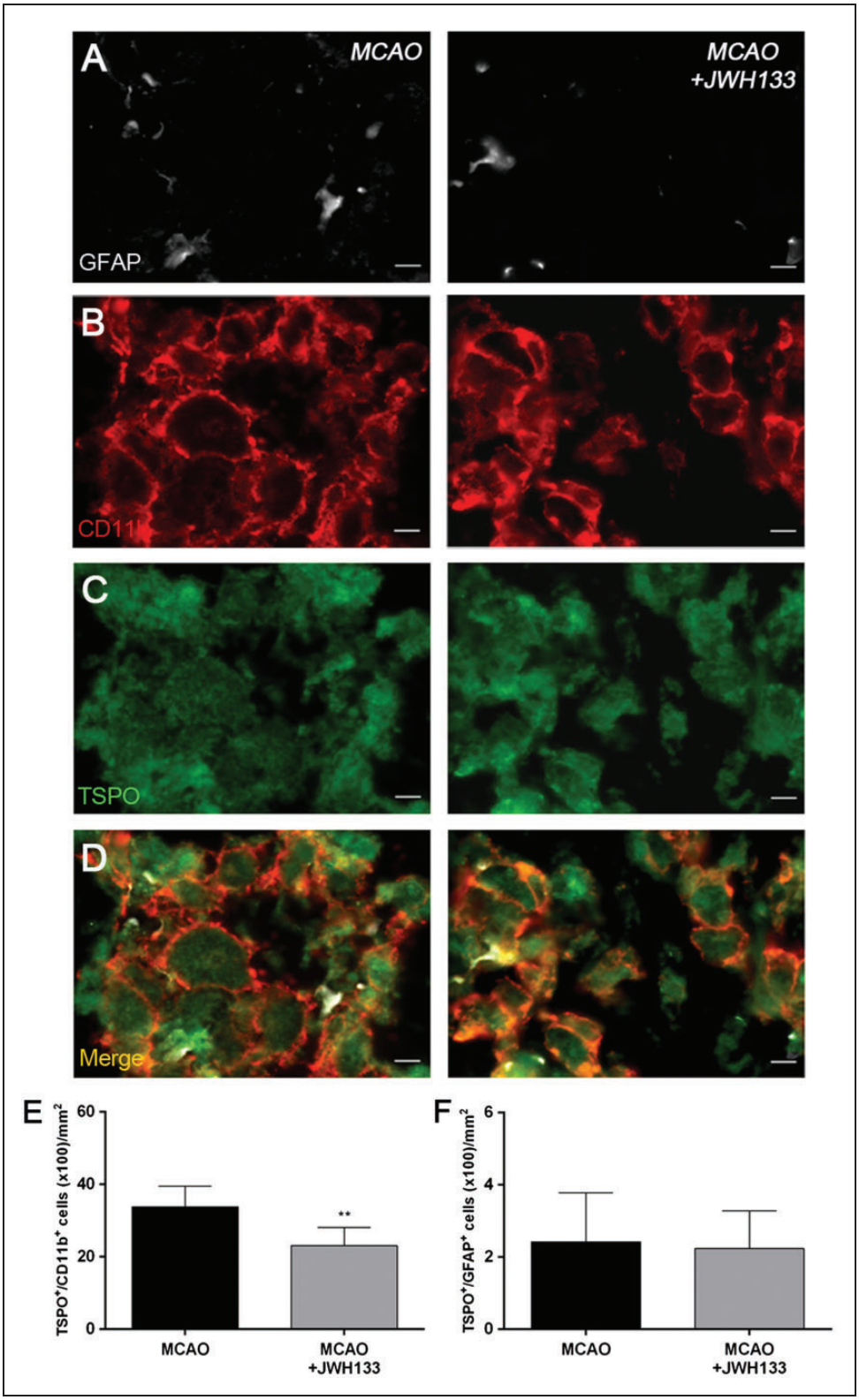

Figure 7. Immunofluorescent labeling of GFAP (white), CD11b (red) and TSPO (green) in the ischemic area, shown as three channels. The data show temporal evolution of TSPO in microglial and astrocytic cells at day 7 after MCAO in vehicle (left column, n = 5) and JWH133-treated rats (right column, n = 7). GFAP-positive astrocytes do not change after treatments (a). CD11b-reactive microglia/macrophages (b) and TSPO receptor (c) decrease after MCAO in JWH133-treated rats. (d) Merged images of three immunofluorescent antibodies. The number of CD11b-reactive microglia/macrophages expressing TSPO decrease at day 7 after daily treatment with JWH133 (e). The number of GFAP-reactive astrocytes expressing TSPO shows similar values following treatment (f). $^{**}p < 0.01$ compared with vehicle. Scale bars, 5 μm.

radiotracers for the in vivo imaging of CB2 receptors may be essential to better understand the role of CB2R in cerebral inflammation. Because of this, we have studied the in vivo expression of CB2 receptors using [^{11}C]A-836339 PET in combination with immunohistochemistry and autoradiography after cerebral ischemia and in two rat models of neuroinflammation, the intrastriatal LPS and the AMPA injection.

PET imaging of CB2 receptors with [^{11}C]A-836339

PET imaging studies with [^{11}C]A-836339 have demonstrated a low background uptake in the normal mouse brain that might improve the visualization of the CB2 receptor expression after a neuroinflammatory response.[22] These findings are consistent with the low [^{11}C]A-836339 PET uptake observed in the control (day 0) rat brain before cerebral ischemia (Figure 1(a)). In the present study, [^{11}C]A-836339 was evaluated from day 1 to 28 after cerebral ischemia to monitor CB2 expression under neuroinflammatory conditions. In the infarcted cerebral hemisphere, [^{11}C]A-836339 showed a non-significant increase in uptake at day 7 after reperfusion followed by binding recovery to pseudo-control values at days 14 to 28 after ischemia (Figure 1(d)). This result was also reflected in the marginally increased time activity curve of [^{11}C]A-836339 in the ipsilateral hemisphere at day 7 in comparison to the control rat brain (Figure 1(f)). Altogether, these findings stand in agreement with Vandeputte and collaborators who, after monitoring CB2 receptors with [^{11}C]NE40 PET following a photothrombotic stroke model, did not observe any significant difference between stroke and sham-operated animals.[24] In fact, these previous results may be explained by the relatively low affinity of [^{11}C]NE40 (Ki 9.6 nM) that might limit its sensitivity for the detection of low concentration of CB2 receptors.[24] [^{11}C]A-836339 displays a significantly higher binding affinity (Ki 0.7 nM) in comparison to [^{11}C]NE40.[22] Our negative results in the ischemic model might suggest that CB2 receptor radioligands with subnanomolar affinity might be required to properly map these receptors in small rodents with PET imaging. Despite this, the use of high doses of radioactivity for high-affinity compounds and typical specific activity of 100 GBq/μmol has been associated with a significant mass of the stable compound that might compromise the specific binding of the radiotracer.[37] Therefore, a radioligand with higher specific binding relative to its non-specific binding and not only a greater affinity would be necessary for improving these limitations.

In view of the negative results obtained for the ischemic rat model, two acute models of neuroinflammation were used to support our findings. [^{11}C]A-836339 PET images did not show any significant uptake increase in the injured striatum after LPS (Figure 3) or AMPA (Figure 4) administration in comparison to the non-lesioned brain hemisphere. These findings were supported by the low [^{11}C]A-836339 uptake observed with in vitro autoradiography in the ipsilateral brain hemisphere after LPS and AMPA injection (Figure 5). As well as this, the spleen, which is considered a potential positive control tissue for the CB2 receptor expression due to its high macrophage population, showed a significant [^{11}C]A-836339 uptake increase relative to brain tissue after LPS and AMPA injection. These results stand in contrast with those shown by Horti et al.[12] who observed specific cerebral [^{11}C]A-836339 PET uptake in the LPS-induced mouse model of neuroinflammation. These differences could be explained by the use of different LPS-treatment dose and protocols; while a single intraperitoneal LPS injection of circa 125 μg was chosen by Horti et al., a 1 μg intracerebral LPS injection was used in our study. Nevertheless, as described by Dickens et al.,[26] this low dose for intrastriatal LPS injection is sufficient to create a neuroinflammatory lesion that can be monitored using TSPO PET radioligands. In fact, autoradiographic studies with [^{18}F]DPA-714 have shown the neuroinflammatory reaction following LPS injection that was not supported by the increase of [^{11}C]A-836339 binding (Figure 5).

Ex vivo CB2 expression after cerebral ischemia, LPS and AMPA administration

Immunohistochemistry confirmed the activation of microglia at day 7 followed by a decrease at day 28 after ischemia onset. These findings confirmed the well-known neuroinflammatory response after 90-min MCAO in rats.[28] Further, CB2 receptors displayed an expression increase, albeit modest, at days 7–28 after reperfusion (Figure 2). These results confirmed that microglia/macrophages partially co-localized with CB2 receptor after cerebral ischemia in rats. Indeed, the low CB2 receptor expression after cerebral ischemia agrees with the lack of specific [^{11}C]A-836339 uptake following experimental stroke in rats. In addition, the low CB2 receptor expression levels after cerebral ischemia have been previously observed during the three days following a photothrombotic model of ischemic stroke in mice.[24] Finally, immunohistochemical studies for the CB2 receptor after LPS and AMPA administration confirmed that CB2 receptors exhibited low expression and co-localization with microglia/macrophages after local injections of LPS (Figure 3) and AMPA (Figure 4). Therefore, the limitations of [^{11}C]A-836339 to image CB2 receptors could be the result of (i) a limitation of the radiotracer for in vivo

imaging detection of these receptors and (ii) the low CB2 receptor expression in the investigated models with a confirmed neuroinflammatory reaction.

CB2 activation attenuates neuroinflammatory response after cerebral ischemia

Pharmacologic CB2 receptor activation with the selective agonists JWH133, O-3853 and O-1966 has been associated with (i) the reduction of white blood cells in both rolling and adhesion to the cerebral vessels, (ii) a decrease of brain lesion size and (iii) the improvement of motor function after cerebral ischemia in mice.[8,10,38,39] In our study, we explored the effect of JWH133 on neuroinflammation by using [^{18}F]DPA-714 PET binding and TSPO immunohistochemistry following cerebral ischemia (Figures 6 and 7). The activation of CB2 receptors with JWH133 induced a significant decrease of the TSPO expression following seven days after reperfusion in microglial cells (Figures 6(e) and (f) and 7(e)). Thus, these results support the role of CB2 receptor on inflammatory reaction following cerebral ischemia in rats. Despite these findings, the treatment with CB2 receptor agonist did not show an improvement in neurological handicap at day 7 after reperfusion relative to the non-treated rats (Figure 6(g)).

Summary and conclusions

We report here [^{11}C]A-836339 PET imaging to assess CB2 receptor expression following cerebral ischemia, LPS and AMPA induced models of neuroinflammation and its relationship with inflammatory response after cerebral ischemia in rats. Our results showed a lack of [^{11}C]A-836339 uptake after stroke, LPS and AMPA injection demonstrating the limitation of this radiotracer to image CB2 receptor under pathological conditions in brain. As well as that, the CB2 receptor displayed a modest expression increase after cerebral ischemia, LPS and AMPA injection by using immunohistochemistry and the activation of CB2 receptors was able to promote a decrease of [^{18}F]DPA-714 uptake and TSPO expression. Therefore, these findings provide novel insights on the usefulness of [^{11}C]A-836339 to monitor in vivo CB2 receptor expression using PET imaging. Future studies should investigate alternative radiotracers that can bind to CB2 receptors following brain inflammation.

Funding

The author(s) disclosed receipt of the following financial support for the research, authorship, and/or publication of this article: This study was funded by the Department of Industry of the Basque Government and Spanish Ministry of Economy and Competitiveness through grant SAF2014-54070-JIN, the EU 7th Framework Programme (FP7/2007-2013) under grant agreement n° 278850 (INMiND) and the France Life Imaging under grant agreement ANR-11-INBS-0006 (FLI).

Acknowledgements

The authors would like to thank L Colas, Dr. B Sczcupak, L Morales, A Leukona, V Salinas, A Arrieta and A Cano for technical support in the immunohictochemistry, radiosynthesis and technical assistance in the PET studies, Dr. C Wimberley for English language editing and Prof. M Higuchi for the gift of the NP155 antibody.

Declaration of conflicting interests

The author(s) declared no potential conflicts of interest with respect to the research, authorship, and/or publication of this article.

Author's contributions

GP, VG-V, DP, AM performed experiments, RB, FD, JLL, AW, AM, designed experiments, AW, AM, FD analyzed data and prepared the manuscript.

References

1. Manzanares J, Julian M and Carrascosa A. Role of the cannabinoid system in pain control and therapeutic implications for the management of acute and chronic pain episodes. *Curr Neuropharmacol* 2006; 4: 239–257.
2. Fernandez-Ruiz J, Moro MA and Martinez-Orgado J. Cannabinoids in neurodegenerative disorders and stroke/brain trauma: From preclinical models to clinical applications. *Neurotherapeutics* 2015; 12: 793–806.
3. Mackie K. Distribution of cannabinoid receptors in the central and peripheral nervous system. *Handb Exp Pharmacol* 2005; 168: 299–325.
4. Cabral GA, Raborn ES, Griffin L, et al. CB2 receptors in the brain: Role in central immune function. *Br J Pharmacol* 2008; 153: 240–251.
5. Miller AM and Stella N. CB2 receptor-mediated migration of immune cells: It can go either way. *Br J Pharmacol* 2008; 153: 299–308.
6. Stella N. Cannabinoid and cannabinoid-like receptors in microglia, astrocytes, and astrocytomas. *Glia* 2010; 58: 1017–1030.
7. Matias I, Pochard P, Orlando P, et al. Presence and regulation of the endocannabinoid system in human dendritic cells. *Eur J Biochem* 2002; 269: 3771–3778.
8. Zarruk JG, Fernandez-Lopez D, Garcia-Yebenes I, et al. Cannabinoid type 2 receptor activation downregulates stroke-induced classic and alternative brain macrophage/microglial activation concomitant to neuroprotection. *Stroke* 2012; 43: 211–219.
9. Nagayama T, Sinor AD, Simon RP, et al. Cannabinoids and neuroprotection in global and focal cerebral ischemia and in neuronal cultures. *J Neurosci* 1999; 19: 2987–2995.
10. Zhang M, Martin BR, Adler MW, et al. Cannabinoid CB(2) receptor activation decreases cerebral infarction in a mouse focal ischemia/reperfusion model. *J Cereb Blood Flow Metab* 2007; 27: 1387–1396.

11. Kong W, Li H, Tuma RF, et al. Selective CB2 receptor activation ameliorates EAE by reducing Th17 differentiation and immune cell accumulation in the CNS. *Cell Immunol* 2014; 287: 1–17.
12. Arevalo-Martin A, Molina-Holgado E and Guaza C. A CB(1)/CB(2) receptor agonist, WIN 55,212-2, exerts its therapeutic effect in a viral autoimmune model of multiple sclerosis by restoring self-tolerance to myelin. *Neuropharmacology* 2012; 63: 385–393.
13. Aso E, Juves S, Maldonado R, et al. CB2 cannabinoid receptor agonist ameliorates Alzheimer-like phenotype in AbetaPP/PS1 mice. *J Alzheimers Dis* 2013; 35: 847–858.
14. Palazuelos J, Aguado T, Pazos MR, et al. Microglial CB2 cannabinoid receptors are neuroprotective in Huntington's disease excitotoxicity. *Brain* 2009; 132: 3152–3164.
15. Sagredo O, Gonzalez S, Aroyo I, et al. Cannabinoid CB2 receptor agonists protect the striatum against malonate toxicity: Relevance for Huntington's disease. *Glia* 2009; 57: 1154–1167.
16. Price DA, Martinez AA, Seillier A, et al. WIN55,212-2, a cannabinoid receptor agonist, protects against nigrostriatal cell loss in the 1-methyl-4-phenyl-1,2,3,6-tetrahydropyridine mouse model of Parkinson's disease. *Eur J Neurosci* 2009; 29: 2177–2186.
17. Shoemaker JL, Seely KA, Reed RL, et al. The CB2 cannabinoid agonist AM-1241 prolongs survival in a transgenic mouse model of amyotrophic lateral sclerosis when initiated at symptom onset. *J Neurochem* 2007; 101: 87–98.
18. Kim K, Moore DH, Makriyannis A, et al. AM1241, a cannabinoid CB2 receptor selective compound, delays disease progression in a mouse model of amyotrophic lateral sclerosis. *Eur J Pharmacol* 2006; 542: 100–105.
19. Mu L, Bieri D, Slavik R, et al. Radiolabeling and in vitro /in vivo evaluation of N-(1-adamantyl)-8-methoxy-4-oxo-1-phenyl-1,4-dihydroquinoline-3-carboxamide as a PET probe for imaging cannabinoid type 2 receptor. *J Neurochem* 2013; 126: 616–624.
20. Slavik R, Herde AM, Bieri D, et al. Synthesis, radiolabeling and evaluation of novel 4-oxo-quinoline derivatives as PET tracers for imaging cannabinoid type 2 receptor. *Eur J Med Chem* 2015; 92: 554–564.
21. Saccomanni G, Pascali G, Carlo SD, et al. Design, synthesis and preliminary evaluation of (18)F-labelled 1,8-naphthyridin- and quinolin-2-one-3-carboxamide derivatives for PET imaging of CB2 cannabinoid receptor. *Bioorg Med Chem Lett* 2015; 25: 2532–2535.
22. Horti AG, Gao Y, Ravert HT, et al. Synthesis and biodistribution of [11C]A-836339, a new potential radioligand for PET imaging of cannabinoid type 2 receptors (CB2). *Bioorg Med Chem* 2010; 18: 5202–5207.
23. Ahmad R, Koole M, Evens N, et al. Whole-body biodistribution and radiation dosimetry of the cannabinoid type 2 receptor ligand [11C]-NE40 in healthy subjects. *Mol Imaging Biol* 2013; 15: 384–390.
24. Vandeputte C, Casteels C, Struys T, et al. Small-animal PET imaging of the type 1 and type 2 cannabinoid receptors in a photothrombotic stroke model. *Eur J Nucl Med Mol Imaging* 2012; 39: 1796–1806.
25. Martin A, Boisgard R, Theze B, et al. Evaluation of the PBR/TSPO radioligand [(18)F]DPA-714 in a rat model of focal cerebral ischemia. *J Cereb Blood Flow Metab* 2010; 30: 230–241.
26. Dickens AM, Vainio S, Marjamaki P, et al. Detection of microglial activation in an acute model of neuroinflammation using PET and radiotracers 11 C-(R)-PK11195 and 18F-GE-180. *J Nucl Med* 2014; 55: 466–472.
27. Chauveau F, Van Camp N, Dolle F, et al. Comparative evaluation of the translocator protein radioligands 11C-DPA-713, 18F-DPA-714, and 11C-PK11195 in a rat model of acute neuroinflammation. *J Nucl Med* 2009; 50: 468–476.
28. Martin A, Szczupak B, Gomez-Vallejo V, et al. In vivo PET imaging of the alpha4beta2 nicotinic acetylcholine receptor as a marker for brain inflammation after cerebral ischemia. *J Neurosci* 2015; 35: 5998–6009.
29. Justicia C, Perez-Asensio FJ, Burguete MC, et al. Administration of transforming growth factor-alpha reduces infarct volume after transient focal cerebral ischemia in the rat. *J Cereb Blood Flow Metab* 2001; 21: 1097–1104.
30. Kuhnast B, Damont A, Hinnen F, et al. [18F]DPA-714, [18F]PBR111 and [18F]FEDAA1106-selective radioligands for imaging TSPO 18 kDa with PET: Automated radiosynthesis on a TRACERLAb FX-FN synthesizer and quality controls. *Appl Radiat Isot* 2012; 70: 489–497.
31. Damont A, Hinnen F, Kuhnast B, et al. Radiosynthesis of [18F]DPA-714, a selective radioligand for imaging the translocator protein (18 kDa) with PET. *J Labell Comp Radiopharm* 2008; 51: 286–292.
32. Sridharan S, Lepelletier FX, Trigg W, et al. Comparative evaluation of three TSPO PET radiotracers in a LPS-induced model of mild neuroinflammation in rats. *Mol Imaging Biol* 2016; 1: 1.
33. Boutin H, Chauveau F, Thominiaux C, et al. 11C-DPA-713: A novel peripheral benzodiazepine receptor PET ligand for in vivo imaging of neuroinflammation. *J Nucl Med* 2007; 48: 573–581.
34. Cizek J, Herholz K, Vollmar S, et al. Fast and robust registration of PET and MR images of human brain. *Neuroimage* 2004; 22: 434–442.
35. Papp EA, Leergaard TB, Calabrese E, et al. Waxholm space atlas of the Sprague Dawley rat brain. *Neuroimage* 2014; 97: 374–386.
36. Menzies SA, Hoff JT and Betz AL. Middle cerebral artery occlusion in rats: A neurological and pathological evaluation of a reproducible model. *Neurosurgery* 1992; 31: 100–106.
37. Hume SP, Gunn RN and Jones T. Pharmacological constraints associated with positron emission tomographic scanning of small laboratory animals. *Eur J Nucl Med* 1998; 25: 173–176.
38. Murikinati S, Juttler E, Keinert T, et al. Activation of cannabinoid 2 receptors protects against cerebral ischemia by inhibiting neutrophil recruitment. *FASEB J* 2010; 24: 788–798.
39. Zhang M, Adler MW, Abood ME, et al. CB2 receptor activation attenuates microcirculatory dysfunction during cerebral ischemic/reperfusion injury. *Microvasc Res* 2009; 78: 86–94.